Applied Physics Letters

Anisotropic magnetic-field-induced phase transition in MnAs nanoribbons

Cite as: Appl. Phys. Lett. **107**, 012407 (2015); https://doi.org/10.1063/1.4926567
Submitted: 27 April 2015 • Accepted: 27 June 2015 • Published Online: 09 July 2015

F. Fernandez Baldis, Martín Sirena, Laura B. Steren, et al.

Anisotropic magnetic-field-induced phase transition in MnAs nanoribbons

F. Fernandez Baldis,[1,2] Martín Sirena,[1,2,a)] Laura B. Steren,[2,3] V. H. Etgens,[4] M. Eddrief,[4] C. Ulysse,[5] and G. Faini[5]
[1]*Centro Atómico Bariloche, Instituto Balseiro–CNEA and Univ. Nac. de Cuyo, 8400 Bariloche, Rio Negro, Argentina*
[2]*Consejo Nacional de Investigaciones Científicas y Técnicas, C1033AAJ Ciudad Autónoma de Buenos Aires, Argentina*
[3]*Centro Atómico Constituyentes, 1650 San Martín, Buenos Aires, Argentina*
[4]*Institut des NanoSciences de Paris, UPMC, CNRS-UMR 7588, 75015 Paris, France*
[5]*LPN-CNRS, Route de Nozay, 91460 Marcoussis, France*

(Received 27 April 2015; accepted 27 June 2015; published online 9 July 2015)

MnAs thin films present a phase coexistence of regularly arranged ferromagnetic (α) and paramagnetic (β) stripes below the Curie temperature when grown onto GaAs(100) substrates. In this letter, we report the observation of a magneto-structural phase transition induced by magnetic field on MnAs nanoribbons below the Curie temperature. A transformation of high-resistance paramagnetic regions into low-resistance ferromagnetic ones is observed above temperature-dependent critical magnetic fields. The phenomenon is hysteretic, highly anisotropic, and size dependent and could be the origin of the high magneto-resistance effect observed at temperatures close to room temperature in these systems. © *2015 AIP Publishing LLC*. [http://dx.doi.org/10.1063/1.4926567]

Promising properties for spintronic[1–4] devices and other applications[5,6] made the study of MnAs thin films a very active topic of development in the last years.[7] Bulk MnAs was known to undergo a first-order magneto-structural transition from a low-temperature hexagonal and ferromagnetic phase (α) to an orthorhombic and paramagnetic one (β) above room temperature (RT).[8] In the ferromagnetic phase, the compound presents a strong uniaxial magnetic anisotropy with the hard-axis aligned to the (0001) axis.

Thin films of MnAs were successfully grown onto various substrates, including semiconductors such as Si and GaAs. Besides the original properties, MnAs films reveal new phenomena arisen from the lattice and thermal expansion mismatch between films and substrates.[9] A coexistence of the α and β phases in a finite temperature range was first reported by Kaganer and co-workers.[10,11] The different orientations of the hexagonal structure onto the substrates define the geometrical arrangement of the α and β phases in the coexistence regime (CR).[2] In the case of MnAs//GaAs (001), the α and β phases forms a periodic array of ferromagnetic and paramagnetic stripes oriented along the MnAs c-axis.[12] Breitwieser *et al.*[13] showed that the period of the α/β stripes pattern, λ, and the height, h, of the α-ridges depend on the film thickness as $\lambda \sim 4.8t$ and $h \sim 0.01t$, respectively. Controlling the number of stripes within the samples at the CR appears to be feasible by confining the films laterally. Moreover, the mean-free path of the electric carriers in MnAs thin films varies from a hundred to a few tenth of nm by changing the films thickness.[14] Magneto-transport experiments turn out to be, so, an excellent tool for the investigation of the phase coexistence regime at the nanoscale.

In this work, we studied the coexistence regime of ferromagnetic and paramagnetic phases on MnAs laterally confined structures through magneto-transport measurements. We found that the resistivity curves at the coexistence regime present in addition to an intrinsic uniaxial anisotropy, particular features associated to the stages of formation and broadening of the α and β stripes. In the same temperature range, an unusual increase of the magnetoresistance ratio together with notable changes of MR curves shape at critical fields are observed. The last results are discussed in the frame of a magnetic field-induced $\beta \rightarrow \alpha$ phase transition. The characteristics of the magnetic transition are investigated by changing different parameters, such as ribbons size and orientation, temperature, and magnetic field. We show that MnAs confined structures exhibit unique features on their magneto-transport properties that are associated to the characteristic lengths of the underlying physics, providing essential information for the development of spintronic devices.

MnAs films were grown by Molecular Beam Epitaxy (MBE) on GaAs(100) substrates as described elsewhere.[15] The films, grown in an As rich atmosphere, accommodate onto the substrates[2,7] with MnAs(1100)//GaAs(100) and MnAs(0001)//GaAs(1–10). Nanoribbons of 20 μm length and variable width were fabricated by e-beam lithography followed by Ar ion milling. In a second step of fabrication, electrical contacts were patterned by optical lithography combined gold deposition and lift-off techniques. The effect of confinement on the α/β phase coexistence was studied by changing the width ($w = 250$ nm and $w = 500$ nm) and thickness ($t = 30$ nm and $t = 300$ nm) of the ribbons. XPEEM measurements performed on similar ribbons showed that the Curie temperature of the samples lays around 320 K and that the hard [0001] uniaxial magnetic anisotropy of the MnAs is preserved in the nanostructures.[16] The anisotropy of the samples' response was investigated by changing the orientation of the wires, i.e., the electrical current axis with respect to the (0001) direction. The electrical current was always applied along the longest side of the wire, either parallel (PA) or perpendicular (PE) to the MnAs c-axis (Figures 1(a) and 1(b)). The field dependence of the longitudinal resistance

a)martin.sirena@hotmail.com

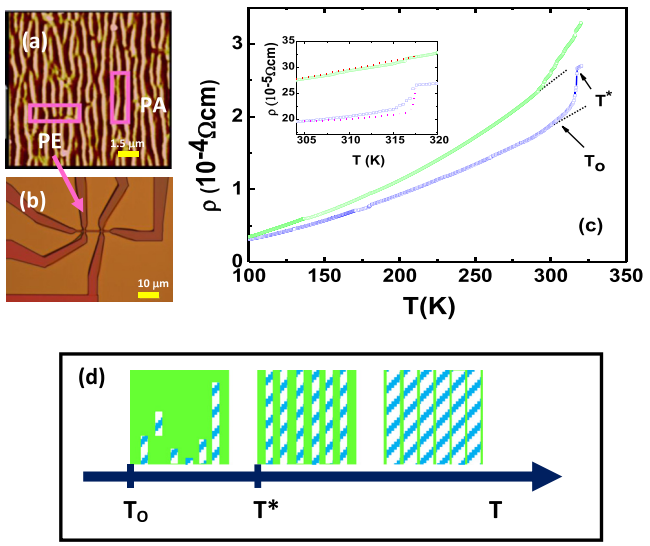

FIG. 1. (a) MFM image of a 300 nm-thick MnAs film, taken at room temperature. Colored rectangles are schemes of the ribbons orientated parallel (PA) and perpendicular (PE) to the c-axis, respectively. (b) SEM image of the magneto-transport device. (c) Resistivity vs. temperature curves for (□) $S500_{PA}$-300 and (o) $S500_{PE}$-300 ribbons. Inset: Detailed of the CR zone including fits of the data (dot lines) following Eqs. (1)–(3). The fitting parameters are ρ_{α}^{PA} (T = 280 K) = 1.95 × 10^{-4} Ω cm, ρ_{α}^{PE} (T = 280 K) = 2.76 × 10^{-4} Ω cm, ρ_{β}^{PA} (T = 320 K) = 2.7 × 10^{-4} Ω cm, ρ_{β}^{PE} (T = 320 K) = 3.28 × 10^{-4} Ω cm, $T_{PE,O} = T_{PA,O} = 280$ K, and T_{PA}*=310 K. (d) Schematic figure of evolution of the α/β phase coexistence as a function of temperature. The paramagnetic phase is described by patterns of diagonal lines.

was measured between 100 K and 320 K with the magnetic field applied perpendicular to the samples surface. The magnetic field sweep was the same for all the measurements and followed this path: 0 T → 9 T → −9 T → 0 T. The samples were indexed as $Sw_{PA(PE)} - t$.

Typical resistivity curves measured for MnAs nanoribbons around the magneto-structural phase transition are shown in Figure 1(c) for the PA and PE geometry. An intrinsic anisotropy, coming from the structural uniaxial symmetry of the MnAs, is clearly distinguished from the curves. The resistivity at the basal plane is higher than along the c-direction at low temperatures in the alpha phase,[17] and this feature is associated to the crystal symmetry of the compound.[18] However, more interesting is the pronounced difference between both curves at the phase-coexistence regime, below the Curie temperature. This "anisotropic behavior" is observed for both series of ribbons, i.e., 30 nm and 300 nm thick, in spite of the fact that the effect is much more noticeable for the thicker samples. In the PA configuration, the resistivity of the ribbons, ρ^{PA}, deviates smoothly from $\rho^{PA}{}_{\alpha}$ as temperature is raised above an onset temperature, T_O, and increases abruptly to $\rho^{PA}{}_{\beta}$ above T*. On the other hand, ρ^{PE} varies almost monotonically from $\rho^{PE}{}_{\alpha}$ to $\rho^{PE}{}_{\beta}$ presenting very small kinks above T_O. This behavior can be understood by analyzing the CR at the different geometries. The stages of formation and growth of the β stripes as the system is warmed play a crucial role in the analysis of the curves. As the MnAs is heated above T_O, a nucleation of the β phase occurs in the ribbons. Once the complete formation of the β stripe occurs, it broadens keeping the same wavelength of the α/β array at the expense of a reduction of the α phase[13] fraction (Fig. 1(d)).

Despite the fact that the CR occurs similarly in both type of samples, the transport across the stripes array depends on the orientation of the stripes with respect to the electrical current.[19] It is also relevant to remark that in thin ribbons ($w \leq \lambda$) no more than a single α/β period can be formed in PA ribbons while several tenths of α/β pairs of stripes will appears in the PE ones along the phase-coexistence temperature range. In the PA configuration, the electrical current is applied parallel to the stripes and so the conduction along the ribbons length, L, is driven in parallel along the α and β stripes channels. In the PE geometry, instead, the current is applied perpendicular to the stripes; the conduction in the sample is the result of a series circuit of α and β stripes. The resistivity of the PA and PE ribbons are modeled taking into account the growth of the relative α/β cross-sectional areas and length of the β stripes as temperature increases. To do so, we assume that the length and width of the β terraces, l_β and w_β, vary[20] with T^2 at the early stage of the α/β phase coexistence while it follows a linear function of T once the stripes are entirely formed and only broaden as the temperature is increased; i.e., $w_\beta = a_w + b_w T^2$ and $l_\beta = a_l + b_l T^2$ for $T_O < T < T^*$ and $w_\beta = a + bT$ for $T^* < T < T_C$. The variation of the stripes size with temperature was modelled after experimental results obtained from X-ray diffraction spectra[11] and resonant X-ray scattering[20] experiments.

The resistivity of the PA configuration is given by

$$\frac{1}{\rho^{PA}} = (1-w_\beta/w)/\rho_\alpha^{PA} + (w_\beta/w)/(\rho_\beta^{PA}.l_\beta/L + \rho_\alpha^{PA}(1-l_\beta/L)) \quad \text{for } T_{PA,O} < T < T_{PA}*, \tag{1}$$

$$\frac{1}{\rho^{PA}} = (1-w_\beta/w)/\rho_\alpha^{PA} + (w_\beta/w)/\rho_\beta^{PA} \quad \text{for } T_{PA}* < T < T_C. \tag{2}$$

While ρ^{PE} is given by

$$\rho^{PE} = N.[\rho_\alpha^{PE}.(\lambda - w\beta)/L + \rho_\beta^{PE}.(w_\beta/L)] \quad \text{for } T_{PE,O} < T < T_C, \tag{3}$$

where N is number of α/β periods. The model was fitted considering the experimental resistivity values of pure α and β phases: ρ_α^{PA} (T = 280 K) = 1.95 × 10^{-4} Ω cm, ρ_α^{PE} (T = 280 K) = 2.76 × 10^{-4} Ω cm, ρ_β^{PA} (T = 320 K) = 2.7 × 10^{-4} Ω cm, ρ_β^{PE} (T = 320 K) = 3.28 × 10^{-4} Ω cm as fixed parameters. The critical temperatures were taken as $T_{PE,O} = T_{PA,O} = 280$ K and $T_{PA}* = 310$ K. We assume that the formation of the stripes along the width of the ribbons occurs in a negligible temperature interval $T_{PE,O} \sim T_{PE}*$ for the calculation of ρ_{PE}. As seen from Figure 1, the model qualitatively describes the temperature variation of the resistivity indicating that the geometric effect of the arrangement of the paramagnetic and ferromagnetic phases at the phase coexistence regime dominate the temperature response of the resistivity. Our results, regarding this "anisotropic behavior" of the resistivity at the CR, contradict previously reported ones. In fact, Takagaki and co-workers did not find any difference of the temperature dependence of the resistivity at the phase-coexistence regime, measured with the current oriented along the [0001] and [11–20] directions.[21,22]

We explain this disagreement by the fact that the MnAs tracks used in the previous papers are much larger than ours and the effect finite size is blurred for these cases.

Magnetoresistance curves at the coexistence regime provides rich information about the magnetization of the ribbons. MR curves measured at different temperatures are plotted in Figs. 2(a)–2(d) for $S500_{PA}$–300 ribbons. The magnetoresistance ratio was defined as $MR\% = (R(H) - R(H=0\,T))/R(H=0\,T) \times 100$. $R(H=0\,T)$ is defined as the resistance measured at zero magnetic field after a complete field cycling ($0\,T \rightarrow 9\,T \rightarrow -9\,T \rightarrow 0\,T$). Below T_O, MR curves are reversible under magnetic field (Fig. 2(a)). The MR effect at the ferromagnetic phase is understood in terms of spin disorder (MR_{SD}). Unexpectedly, as the temperature is raised, two additional contributions are distinguished from the curves. On one hand, the virgin-state (VS) resistivity of MnAs nanoribbons, $R(H=0\,T,VS)$, differs notably from $R(H=0\,T)$, measured after cycling the system to 9 T. As the VS resistivity depends on the α-MnAs/β-MnAs fraction ratio, $\xi(T)$, a positive resistance difference $\Delta R_{VI\text{-}0} = R(H=0\,T,VS)\text{-}R(H=0\,T)$ would indicates that a transformation of a fraction of the β phase into α takes place in the samples as a magnetic field is applied to them. The virgin state is never recovered after magnetic field cycling, suggesting that at least part of the transition from one phase to the other is irreversible with respect to magnetic field. However, a relaxation of $R(H=0\,T)$ towards the VS value is also observed; this could indicate that part of the ferromagnetic fraction created after applying a magnetic field is metastable. $R(H=0)$ varies after a wait time of several minutes, reducing $\Delta R_{VI\text{-}0}$ and indicating that as time goes through, a part of the α phase transforms back to the β phase. A more complete study about the magnetic relation in these systems are needed in order to correctly weigh these two components. Additionally, the $\Delta MR_{VI\text{-}0} = \Delta R_{VI\text{-}0}/R(H=0\,T) \times 100$ ratio is only finite in a narrow temperature range above T_O (Fig. 3(a)) and at magnetic fields higher than $H^*_{VI\text{-}O}$. In Fig. 3(b), the magnetic-field range where the resistance drops is observed in virgin curves and are indicated for different temperatures. The progressive increase of the critical fields as the temperature is raised stresses the higher energy cost of the transformation of β phase into α one, as the system approaches T_C.

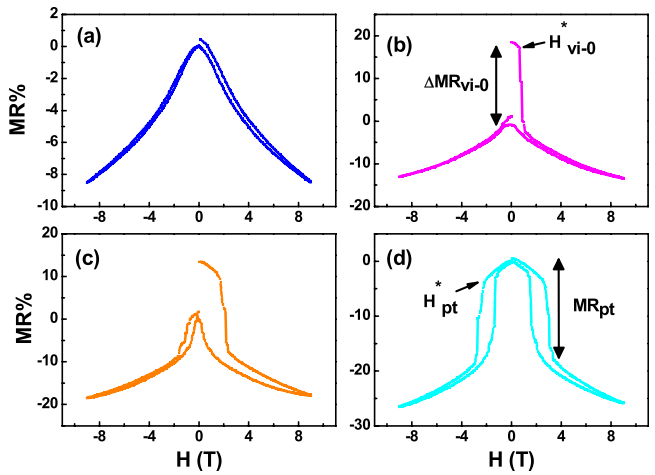

FIG. 2. Magnetoresistance curves of the $S500_{PA}$-300 ribbon measured at (a) $T = 280\,K$, (b) $T = 300\,K$, (c) $T = 315\,K$, and (d) $T = 320\,K$, respectively. The magnetic field sweep in all the measurements followed the same steps: $0\,T \rightarrow 9\,T \rightarrow -9\,T \rightarrow 0\,T$.

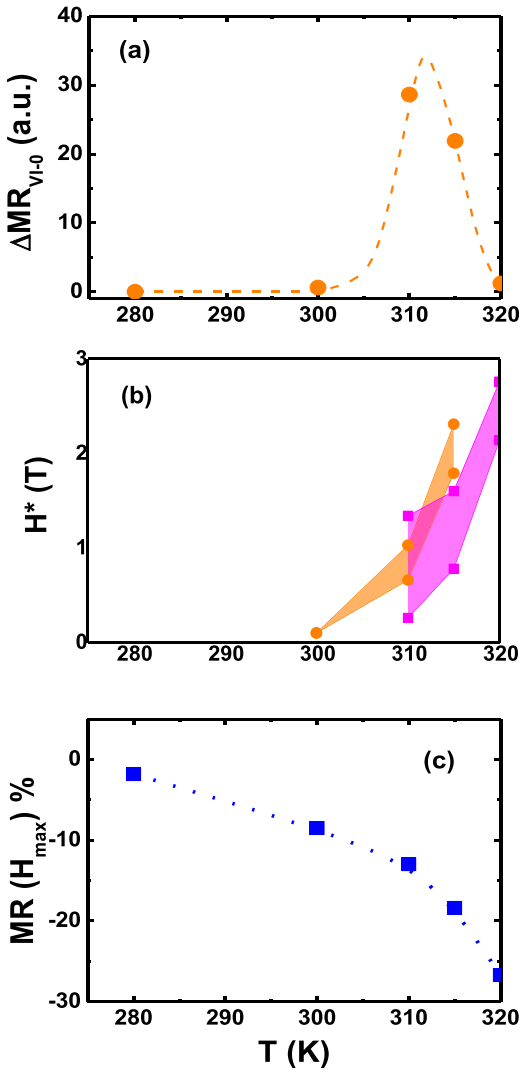

FIG. 3. (a) $\Delta R_{VI\text{-}0}$ vs. T, (b) H* vs. T, extracted from the (●) initial MR curve, H^*_{VI}, and (■) after magnetic field cycling, H^*_{PT}; and (c) MR ratio vs. T. All these values were determined from the MR curves of the $S500_{PA}$-300 ribbon.

On the other hand, a negative and hysteretic magnetoresistance term, MR_{PT}, is measured for fields larger than $H^*_{PT\text{-}O}$, above $T \sim T^*$ (Figs. 2(b)–2(d)). This contribution is reversible with magnetic field and increases by discrete jumps from $H^*_{PT\text{-}O}$ up to a critical saturation field $H^*_{PT\text{-}SAT}$ (Fig. 3(b)).

The maximum MR ratio reaches values of more than 20% around 320 K, superimposing MR_{PT} with MR_{SD}. The temperature dependence of MR presents an unusual increase as the temperature is raised above T_O (Fig. 3(c)). A similar behavior was observed in films[23] and bulk MnAs.[24] Mira *et al.* correlates the increase of the MR to a magnetic-field phase-induced structural transition measured by neutron diffraction experiments. Magnetotransport measurements in lateral confined nanostructures, indicating sharp resistance steps for certain critical fields, seem to corroborate this hypothesis. Additionally, it should be noticed that the critical fields observed for the bulk samples by Mira *et al.* by the

neutron diffraction experiments correspond with the values observed in this work. However, magnetotransport measurements in MnAs nanoribbons reveal additional and unique characteristics about the phase transition which is only detectable in confined structures. Non-zero $\Delta R_{VI\text{-}0}$ and the appearance of MR_{PT} reveal that there are two distinct processes of $\beta \rightarrow \alpha$ magnetic-field induced phase transition. A phase transition irreversible in magnetic field above T_O enhances the original $\xi(H = 0, T)$ by $\xi^{irr}(H^*, T)$. This process takes place at the early β-stripe formation stage in a finite temperature range and relaxes towards the initial ξ ratio after a finite wait time in the absence of magnetic field. Progressively, as the temperature increases, the α/β stripes' assembly is formed in a second process and above $T \sim T^*$ the magnetic field can only broaden the magnetic stripes at the expenses of the paramagnetic one reversibly. The initial ξ is recovered after field cycling. The activation energies for both processes are different and are obtained from Fig. 3(b). In fact, the plot of the critical fields extracted from the MR curves provides another evidence for the recognition of the two processes. In both cases, the critical fields increase with temperature. This behaviour is understood by the fact that the β phase becomes more stable with temperature. As a consequence, the energy cost of the phase transition increases with increasing temperature.

A strong difference between the magnetoresistance vs. field curves measured in the PA and PE configuration is found (Figs. 4(a) and 4(b)). While a few of well-defined resistance jumps are measured for PA samples, curves measured in the PE geometry exhibit a smoother change of resistance as the magnetic field is increased. Small resistance drops are measured for $S500_{PE}$–*300* ribbons as the magnetic field increases above $H^*_{PT\text{-}O} \sim 0.2$ T for 300 K. The threshold field increases with increasing temperatures as found for PA samples. However, while the MR_{PT} of PA samples saturates around 3 T, in the PE ribbons, the MR_{PT} curves are far from saturation at 9 T. The decrease of the resistance with magnetic field at many kinks for PE ribbons is ascribed to the existence of a large number of stripes and so a large distribution of activation energies for the nucleation and broadening of magnetic stripes. The different behavior of the MR curves for the parallel and perpendicular configurations has a parallelism with the "anisotropic behavior" of the temperature dependence of the resistivity at the CR. In both cases, the relevant parameters are the number of periods of the α/β multilayer and the orientation of the stripes with respect to the electrical current.

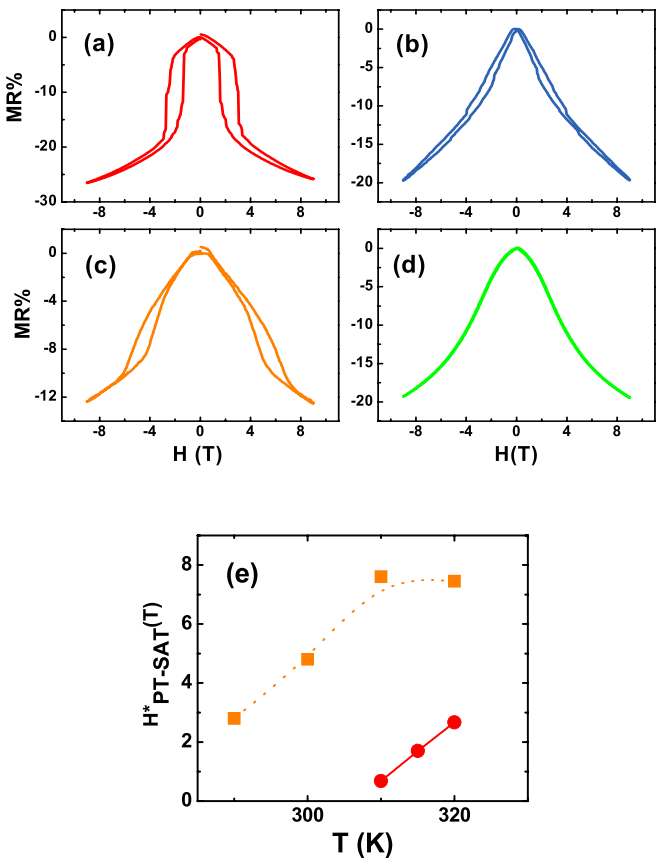

FIG. 4. MR curves of (a) $S500_{PA}$-300, (b) $S500_{PE}$-300, (c) $S250_{PA}$-300, and (d) $S500_{PA}$-30 ribbons measured at T = 320 K. (e) $H^*_{PT\text{-}SAT}$ vs. T for (●) $S500_{PA}$-300 and (■) $S250_{PA}$-300. The magnetic field sweep is as follows: 0 T → 9 T → −9 T → 0 T.

In order to look at the effect of lateral confinement on the field-induced $\beta \rightarrow \alpha$ transition, $S500_{PA}$–*300* and $S250_{PA}$–*300* ribbons were investigated (Figs. 4(a) and 4(c)). The shape of the MR curves is similar for both ribbons, but the critical magnetic fields change (Fig. 4(e)): they increases notably as the samples become narrower. These results indicate that lateral borders affect the pinning of the different phases, increasing the activation energy for the phase-transition as the samples are laterally confined to the nanoscale.

We explore the variation of the effect with samples thickness in order to examine structures with different corrugation, i.e., height of the terraces and α/β periodicity. As seen in Figs. 4(a) and 4(d), the shape of the MR curves is strongly affected by thickness reduction: the resistance jumps disappear in the thinner samples and a smooth variation of R(H) is measured instead. The MR curves resemble those related to spin-disorder effects. It should be noticed that the increase of the MR as a function of temperature for thinner samples, the same as the one observed for the thicker samples, seems to indicate that a $\beta \rightarrow \alpha$ magnetic-field induced phase-transition is still present for these samples. However, the effect of the uniaxial symmetry of α/β phases arrangement onto the transport properties is blurred in very thin ribbons and the MR curves resembles those of α/β disordered structures or bulk compound.[23] This could be related to a reduction of a characteristic length in these systems (compared with the lateral confinement). Indeed, reducing the thickness from 300 nm to 30 nm should induce a change of λ from 1.44 μm to 0.144 μm and a reduction of the height of the ridges from 3 nm to 0.3 nm. The temperature and field dependence of the resistivity of the thinner films suggest that the long-range order of the stripe array is at least partially lost as thickness is reduced below 50 nm, keeping however the symmetry of the phase arrangement. This is consistent with a short-range order of α and β stripes reported for 30 nm films by Ryu and co-workers.[25]

MnAs thin films are interesting candidates for the fabrication of spintronics devices, presenting an excellent growth over semiconductor substrates and an important magnetoresistance effect at room temperature. Magneto-transport

experiments indicate that a paramagnetic to ferromagnetic phase transition is induced in MnAs nanoribbons by the application of a magnetic field. The phase-induced transition was found to be magnetic history and temperature dependent. The critical fields as well as the temperature range at which the phenomenon is observed are notably affected by lateral and vertical confinement. This effect seems to be the origin of the high magnetoresistance effect observed in MnAs thin films for temperatures close to room temperature. Studying the influence of the confinement in these systems is critical for the development of spintronics devices at the nanoscale.

L.B.S. thanks C. Helman for fruitful discussions and acknowledges support from PICT 1187 FONCYT, UNCuyo06/C395, and PIP112-201101-00482 CONICET. L.B.S., F.F.B., V.H.E., and M.E. are members of the Laboratorio Internacional Franco-Argentino en Nanociencias (LIFAN). M.S. acknowledges the financial support from the international cooperation programs PICS level 2 CNRS/CONICET and the PEOPLE MARIE CURIE ACTIONS, International Research Staff Exchange Scheme, Call: FP7-PEOPLE-2012-IRSES, COEF-magNANO.

[1]M. Tanaka, Semicond. Sci. Technol. **17**, 327 (2002).
[2]Y. Takagaki and K.-J. Friedland, J. Appl. Phys. **101**, 113916 (2007).
[3]M. E. Nowakowski, G. D. Fuchs, S. Mack, N. Samarth, and D. D. Awschalom, Phys. Rev. Lett. **105**, 137206 (2010).
[4]M. Tortarolo, L. Thevenard, H. J. von Bardeleben, M. Cubukcu, V. Etgens, M. Eddrief, and C. Gourdon, Appl. Phys. Lett. **101**, 072408 (2012).
[5]C. Spezzani, E. Ferrari, E. Allaria, F. Vidal, A. Ciavardini, R. Delaunay, F. Capotondi, E. Pedersoli, M. Coreno, C. Svetina *et al.*, Phys. Rev. Lett. **113**, 247202 (2014).
[6]J.-Y. Duquesne, J.-Y. Prieur, J. A. Canalejo, V. H. Etgens, M. Eddrief, A. L. Ferreira, and M. Marangolo, Phys. Rev. B **86**, 035207 (2012).
[7]L. Däweritz, Rep. Prog. Phys. **69**, 2581 (2006).
[8]C. P. Bean and D. S. Rodbell, Phys. Rev. **126**, 104 (1962).
[9]L. Daweritz, J. Cryst. Growth **227**, 834 (2001).
[10]V. M. Kaganer, B. Jenichen, F. Schippan, W. Braun, L. Daweritz, and K. H. Ploog, Phys. Rev. Lett. **85**, 341 (2000).
[11]V. M. Kaganer, B. Jenichen, F. Schippan, W. Braun, L. Däweritz, and K. H. Ploog, Phys. Rev. B **66**, 045305 (2002).
[12]A. K. Das, C. Pampuch, A. Ney, T. Hesjedal, L. Daweritz, R. Koch, and K. H. Ploog, Phys. Rev. Lett. **91**, 087203 (2003).
[13]R. Breitwieser, F. Vidal, I. L. Graff, M. Marangolo, M. Eddrief, J.-C. Boulliard, and V. H. Etgens, Phys. Rev. B **80**, 045403 (2009).
[14]K.-J. Friedland, M. Kastner, and L. Daweritz, Phys. Rev. B **67**, 113301 (2003).
[15]L. B. Steren, J. Milano, V. Garcia, M. Marangolo, M. Eddrief, and V. H. Etgens, Phys. Rev. B **74**, 144402 (2006).
[16]M. Tortarolo, F. Fernandez Baldis, M. Sirena, L. B. Steren, J. Milano, V. H. Etgens, M. Eddrief, and G. Faini, J. Appl. Phys. **112**, 013915 (2012).
[17]G. Bodecker, H. Berg, K. Funke, and K. Barner, Phys. Lett. A **78**, 205 (1980).
[18]C. Helman, J. Milano, L. Steren, and A. M. Llois, J. Magn. Magn. Mater. **320**, e415 (2008).
[19]P. L. Rossiter, *The Electrical Resistivity of Metals and Alloys, Cambridge Solid State Science Series* (Cambridge University Press, New York, 1991), p. 170.
[20]R. Magalhães-Paniago, L. N. Coelho, B. R. A. Neves, H. Westfahl, F. Iikawa, L. Daweritz, C. Spezzani, and M. Sacchi, Appl. Phys. Lett. **86**, 053112 (2005).
[21]Y. Takagaki, L. Däweritz, and K. H. Ploog, Phys. Rev. B **75**, 035213 (2007).
[22]Y. Takagaki, C. Hermann, J. Herfort, C. Hucho, and K.-J. Friedland, Phys. Rev. B **78**, 235207 (2008).
[23]J. J. Berry, S. J. Potashnik, S. H. Chun, K. C. Ku, P. Schiffer, and N. Samarth, Phys. Rev. B **64**, 052408 (2001).
[24]J. Mira, F. Rivadulla, J. Rivas, A. Fondado, T. Guidi, R. Caciuffo, F. Carsughi, P. G. Radaelli, and J. B. Goodenough, Phys. Rev. Lett. **90**, 097203 (2003).
[25]K.-S. Ryu, J. Kim, Y. Lee, H. Akinaga, T. Manago, R. Viswan, and S.-C. Shina, Appl. Phys. Lett. **89**, 232506 (2006).